Front. Phys. China, 2008, 3(2): 173–180
DOI 10.1007/s11467-008-0013-3

REVIEW ARTICLE

**Rao HUANG, Li-bo MA, Jian-ping YE,
Yong-qian WANG, Ze-xian CAO**

# Synthesis and photoluminescence studies of silicon nanoparticles embedded in silicon compound films

© Higher Education Press and Springer-Verlag 2008

**Abstract** High-density silicon nanoparticles with well-controlled sizes were grown onto cold substrates in amorphous $SiN_x$ and SiC matrices by plasma-enhanced chemical vapor deposition. Strong, tunable photoluminescence across the whole visible light range has been measured at room temperature from such samples without invoking any post-treatment, and the spectral features can find a qualitative explanation in the framework of quantum confinement effect. Moreover, the decay time was for the first time brought down to within one nanosecond. These excellent features make the silicon nanostructures discussed here very promising candidates for light-emitting units in photonic and optoelectronic applications.

**Keywords** silicon nanoparticles, photoluminescence, quantum confinement effect

**PACS numbers** 78.55.Ap, 78.67.Bf, 78.47.Cd

## 1 Introduction

Silicon-based light-emitting structures are likely to provide the pivotal technology in future full-silicon optoelectronic integration. Unfortunately bulk silicon is an indirect bandgap ($E_g$ ~1.12 eV) semiconductor which emits light at a negligibly low efficiency. Since the first discovery of visible photoluminescence (PL) from porous silicon at room temperature by Canham in 1990 [1], arduous efforts have been made to squeeze light from silicon, and a great multitude of exciting results, both theoretical and experimental, concerning the optical and electronic properties of diversified structures have been acquired [2−9].

For a long period, the fabrication of nanostructured systems which are expected to give appreciable light emission following the quantum confinement effect (QCE) [3, 5, 9], as confirmed in size-separated silicon nanoparticles [2], has attracted much research interest. Various silicon based structures have been investigated in an effort to obtain applicable light emission. These include, for instance, Si nanocrystals in amorphous silicon matrix [3], free-standing film of silica containing Si nanocrystals [9], silicon nanoparticles embedded in a diamond matrix [10], and so forth. So far, PL in the spectral range from infrared to even ultraviolet has been registered in many silicon nanostructures.

As one of the workhorse materials for microelectronics, silicon oxide is the most widely studied among the various matrix choices to quantum confine silicon nanoparticles which are intended to be made into efficient emitting centers. However, the ultimate goal of silicon-based light emitting material design is not the realization of photoluminescence but to obtain applicable electroluminescence. Therefore, carrier injection through the insulating matrix (clearly only possible via the tunneling mechanism) is of practical concern. In this sense, $SiO_2$ is obviously a bad choice because of its extremely large bandgap ($E_g \sim 8.5$ eV) — the operation voltage for a light-emitting diode based on Si-in-$SiO_2$ structure would be unacceptably high. To circumvent this difficulty for later implementations, and also to explore the light emission properties

Rao HUANG[1], Li-bo MA[1], Jian-ping YE[2], Yong-qian WANG[1], Ze-xian CAO[1] (✉)

[1] Beijing National Laboratory for Condensed Matter Physics, Institute of Physics, The Chinese Academy of Sciences, P. O. Box 603, Beijing 100080, China
[2] Key Laboratory of Photochemistry, Institute of Chemistry, The Chinese Academy of Sciences, P. O. Box 2709, Beijing 100080, China
E-mail: rhuang@aphy.iphy.ac.cn; zxcao@aphy.iphy.ac.cn

*Received January 3, 2008; accepted January 20, 2008*

of silicon nanoparticles embedded in other materials, the compounds of nonstoichiometrical silicon nitride ($E_g \sim$ 5.0 eV), denoted as $SiN_x$, and the stoichiometrical SiC ($E_g$ ranging from ~2.3 to 3.4 eV. For the amorphous SiC concerned here, it is ~3.2 eV) have been employed and the PL from such composite nanostructures has been extensively investigated in recent years.

In this article, we present a brief review of the progresses along the line of fabricating Si-in-$SiN_x$ and Si-in-SiC nanostructures to obtain intense and tunable light emissions via QCE. By using a low-temperature growth procedure, the sizes of the silicon nanoparticles can be reduced down to ~1.2 nm, and the external quantum efficiency of PL thereof amounts to over 3.0 %. Moreover, the decay time has been reduced to within one nanosecond.

## 2 Experimental details

The Si-in-$SiN_x$ and Si-in-SiC composite films were deposited onto single-crystalline Si (100) wafers by a custom-designed capacitance-coupled PECVD setup (Fig. 1) operated at an RF power of 35 W and at a typical working pressure of $3.0\times10^{-1}$ mbar. Precursors are a gas mixture of high-purity $SiH_4$ (diluted with $H_2$ to 2.0 vol. %) and $H_2$ with the addition of $N_2$ for the nitride and of $CH_4$ for the carbide system, respectively. No intentional substrate heating was applied, thus the substrate temperature was maintained at below 60 °C by end of deposition. The film thickness can be controlled by varying the growth time; it generally spans a range of 0.5−1.5 μm. As to the size of the silicon nanoparticles, it can be well controlled by adjusting the plasma conditions through changing the total pressure, the power density and/or the fraction of silane in the precursor, therefore the relevant parameters will be specified at places where it is proper.

The local atomic environments and bonding configurations in the deposits were characterized by infrared absorption measurement performed on a Perkin-Elmer 2000 Fourier-transform infrared system and by inspecting the Si 2p line excited with Mg $K_\alpha$ radiation on an X-ray photoelectron spectrometer (ESCALab Mark-II). Formation of silicon nanocrystals in the films was also verified by micro-Raman scattering using a confocal laser Raman spectrometer (JY-6400). The size and spatial distribution of the innate silicon nanoparticles were investigated from bright-field images obtained with a Tecnai-20 transmission electron microscope (TEM), for which a proper defocus value had to be chosen to accomplish an enhanced contrast. Size determination suffers from a large uncertainty due to the amorphous nature of the silicon particles and the less pronounced particle/matrix absorption contrast.

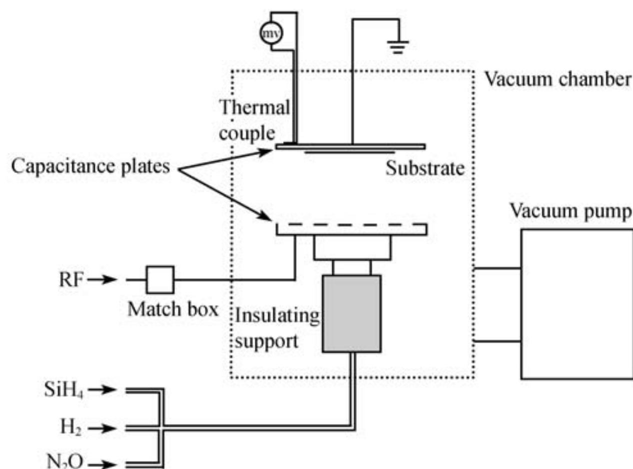


**Fig. 1** A custom-designed capacitance-coupled PECVD setup. Plate diameter $\phi = 100$ mm.

The as-deposited films would be first examined under an ultraviolet lamp to confirm the presence of PL. Room-temperature PL measurements were carried out on an FLS 920 (Edinburgh Instruments Ltd.) fluorescence spectrometer with a xenon lamp as excitation source. Time-resolved analysis was made on a spectrophotometer (Horiba NAES-1100) with the excitation at 375 nm from a hydrogen lamp (chopper frequency 10 kHz, pulse width 2.0 ns) to determine the decay times at different emission wavelengths registered within less than 1.0 nm. The temporal resolution of the SSU-112 photomultiplier employed is 0.1 ns. As to the external quantum efficiency, it was determined by spectrophotometric measurement with the aid of an integrating sphere which collects both reflected and emitted light without wavelength discrimination. Other parameters or methods associated with the preparation or characterization of a particular sample will be indicated where needed.

## 3 Si-in-$SiN_x$ compound films

By varying the nitrogen-to-silane flow rate ratio between 1.0 and 5.5, we deposited a group of Si-in-$SiN_x$ films. Grown under conditions favorable for the formation of distinct silicon particles, the matrix material silicon nitride is generally slightly nitrogen-deficient, that's why we employ the notation $SiN_x$. According to the X-ray photoelectron spectroscopic and electron energy loss spectroscopic characterizations, the "$x$" value was found to change only slightly, scattering around 1.10.

The morphology of the as-deposited Si-in-$SiN_x$ films

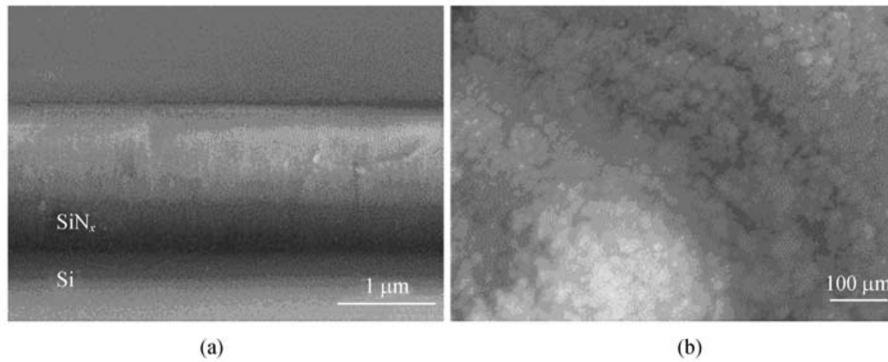


**Fig. 2** SEM micrographs exhibiting the cross section **(a)** and surface **(b)** morphology of an amorphous Si-in-SiN$_x$ compound film.

was revealed by the SEM micrographs exemplified in Fig. 2. Seen from the cross section and plan view, the film exhibits a compact surface morphology and assumes a good adhesion to the substrate.

The presence of silicon particles in the films can be confirmed by IR absorption measurement and/or by the occurrence of the 520 cm$^{-1}$ peak on the Raman spectrum. From the high-resolution TEM micrograph (Fig. 3) of a sample grown with gas flow rates (in sccm) $SiH_4$:$N_2$:$H_2$=8.0: 8.0:10, we see that silicon nanoparticles with sharp boundaries are homogeneously distributed throughout the film, with an average size of about 1.8 nm. The density of silicon particles amounts to about $1.07\times10^{13}/cm^2$. Because of the very high number density, some weakly connected clusters of particles have been observed. The particles are quite uniform in size with only a slight fluctuation.

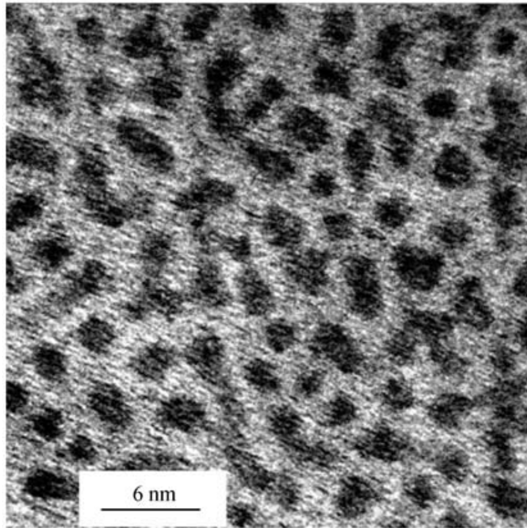


**Fig. 3** High-resolution TEM micrograph revealing the amorphous silicon particles embedded in the SiN$_x$ matrix with slight size fluctuation and sporadic weak interconnections. Averaged particle size is about 1.8 nm.

The Si-in-SiN$_x$ films prepared with the aforementioned procedure can emit strong blue-violet light which can be easily detected at room temperature. In Fig. 4, the PL spectrum of an as-deposited compound film was displayed against that from a single crystalline GaN sample both excited by the 325 nm line from a He-Cd laser. In comparison with GaN, a remarkable feature for the PL spectrum of the Si-in-SiN$_x$ film centered at 428 nm was its relatively enormous width, though their integral intensities were roughly equal. The full width at half maximum (FWHM) is 70 nm for the Si-in-SiN$_x$ sample which corresponds to a half-width of 0.47 eV in photon energy, indicating a relatively serious effect of size fluctuation for particles that small.

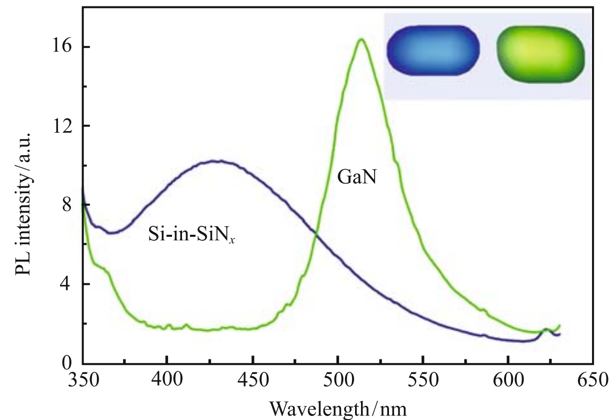


**Fig. 4** PL of the Si-in-SiN$_x$ deposit with an overall atomic ratio [N] / [Si]∼0.77 plotted against that from a single crystalline GaN sample. Inset shows the digital photo of the two films under illumination of a 6-W ultraviolet lamp. The Si-in-SiN$_x$ sample (*left*) is in blue.

For the sample containing silicon particles of about 1.8 nm in size, Fig. 5 plots PL profiles obtained under various excitation wavelengths, and the spectral features including the peak position, integral intensity and the full-width-at-half-maximum as functions of the excitation wavelength. The fine-scan PL spectra were achieved with an excitation wavelength between 300 and 450 nm (4.1−2.8 eV) at room temperature. No

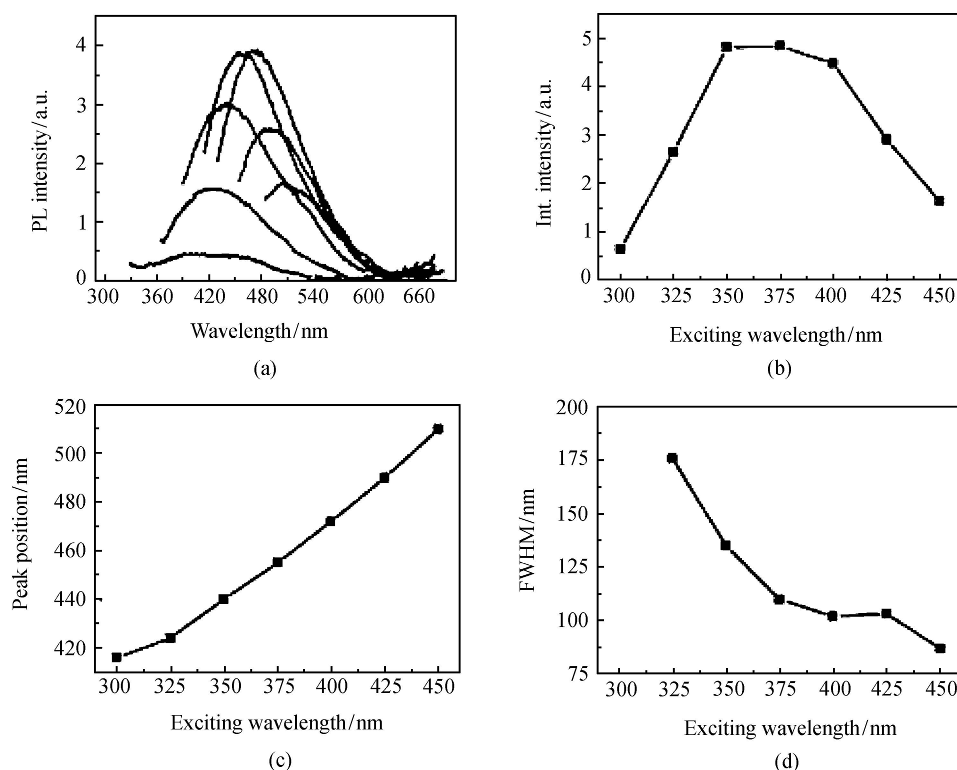


**Fig. 5** **(a)** PL profiles measured at an excitation wavelength (from left to right) varied from 300 to 450 nm at a step length of 25 nm. The integral intensity, peak position and FWHM are presented as functions of the excitation wavelength in **(b)**, **(c)** and **(d)**, respectively.

strong PL can be detected under excitations beyond this range. The emission profile excited by the 300 nm line even extends considerably to below 400 nm, and at the excitation wavelength of 450 nm the peak position of the emission has been approximately shifted, in a roughly linear manner, from 416 to 510 nm [Fig. 5 (a),(b)]. The spectral profiles possess a quite standard Gaussian shape when displayed accordingly versus the photon energy, which facilitates the calculation of the integral intensity and the spectral width from the incomplete emission spectra due to the cut-off at the short-wavelength side. From the curve for the integral intensity variation [Fig. 5(c)], we see that the most effective excitation occurs at ~375 nm, as confirmed by the PL excitation spectrum monitored at an emission wavelength of 455 nm (not shown here, see Ref. [11]). Remarkably, a plateau of emission integral intensity appears within 340 to 410 nm. This implies an enormous flexibility in choosing the excitation source and the emitted wavelengths for applications. The FWHM of the PL profiles increases rapidly at shorter excitation wavelength [Fig. 5(d)]. The data point at 300 nm is unreliable because of the poor profile quality for the very weak emission]. This is quite understandable in the scenario of QCE. The PL under a shorter excitation wavelength clearly involves more particles of smaller sizes, to which an equally large size fluctuation implies an enhanced fluctuation in the energy for the emitted photons. The effect is obviously more pronounced, and asymmetrical, when the spectrum is displayed versus wavelength.

The external quantum efficiency was determined by spectrophotometric measurements using an integrating sphere which collects both the reflected and emitted light of longer wavelength without wavelength discrimination. In Fig. 6, the spectrum of reflectance was measured with a separate spectrometer in a differing wavelength range. The strong multiply-reflected light beam inside the integrating sphere also excited PL from other parts than the sample, resulting in a disturbing contribution to the collected intensity which has to be extracted by the calculation of external quantum efficiency. This disturbing contribution can roughly be calibrated with the same measurements in a stoichiometric $Si_3N_4$ sample (not shown here), which exhibits a difference of 6.0 % for the two curves (in percentage of the incident intensity) at the pumping wavelength of 600 nm, where no PL from either the stoichiometric or the nanostructured samples is expected. At 325 nm, for example, the difference between the collected intensity and the reflected intensity is 4.9 %, being slightly less than that at 600 nm. Ac-

cordingly, in order to make a cautious estimation of the external quantum efficiency, we assume the same value for the disturbing contribution to the collected intensity at the pumping wavelength of 325 nm as that at 600 nm, i.e., 5.3 % as read from the curves at 600 nm (Fig. 6). At 325 nm, the difference between the collected intensity and the reflected light is about 11.5 %. Taking off the contribution of irrelevant PL, this implies a power ratio of $I_{\mathrm{PL}}/I_{\mathrm{incident}}$ ≈6.2 %. From the formula $\eta_{\mathrm{PL}} = C^{*}(I_{\mathrm{PL}}\lambda_{\mathrm{incident}}/\ I_{\mathrm{incident}}\bar{\lambda}_{\mathrm{PL}})$, where $\bar{\lambda}_{\mathrm{PL}} \approx 428$ nm is the weight averaged wavelength of PL, and $C$ is a correction factor for the varying detector sensitivity. $C$ is assigned a value of about 0.5, bearing in mind that the PL centers at 428 nm, while the detector manifests a doubled sensitivity at 550 nm than at 325 nm. An external quantum efficiency of over 3.0 % can be consequently derived.

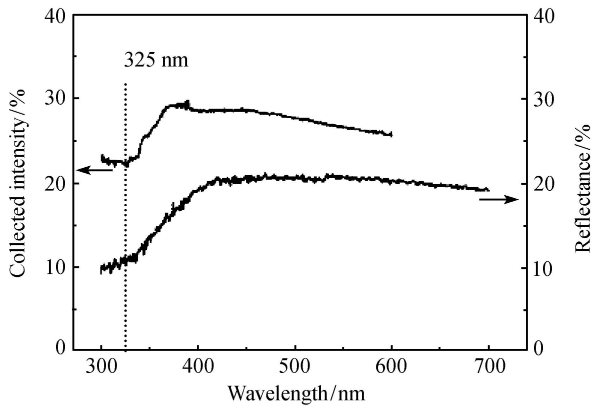


**Fig. 6** Reflectance (*lower curve*) of the Si-in-$SiN_x$ sample plotted as a function of exciting wavelength against that of the integral intensity (*upper curve*) containing contributions from both the reflected and the emitted light.

Time-resolved analysis revealed a very short radiative lifetime in the order of 1.0 nanosecond for the Si-in-$SiN_x$ sample concerned here, which is in strong contrast to the porous silicon where the typical decay times for emission are generally in milliseconds. Figure 7 displays an emission spectrum under the excitation of the 375 nm line, together with the decay times for the emissions at various wavelengths. The decay times are the results of fitting the decaying process (see the inset) with a double exponential decaying function, thus there is a long decay time attribute and a short decay time attribute. Such a fitting procedure has been employed by many researchers [12], to which the tacit assumption is that two decaying paths are responsible for the decaying process. In a model proposed by Calcott *et al.* [13] for porous silicon, it states that the electron — hole exchange interaction splits the excitonic levels by an energy $D$ due to quantum confinement, and the upper level (a triplet state) and the lower level (a singlet state) have different radiative decay rates [14]. This model has also been applied to silicon nanoparticles [15, 16]. Following this model, the energy difference $D$ is expected to be about a few tens of meV, and the difference in the decay times can be by a factor of 10 in the range of a nanosecond when the silicon particles are about 2.0 nm large, as predicted by Leung [16]. We see that both the long and short decay times — they differ roughly by a factor within 10 — decrease at longer emission wavelengths, i.e., the decay time is emission wavelength-dependent as found in porous silicon [17]. Across the emission spectrum, even the long decay times (of roughly the same value as the decay time from the fitting result by using a stretched exponential decaying function) are less than 1.0 ns. This very sensitive response to optical excitation holds potential for the fabrication of silicon-based devices to operate at gigahertz.

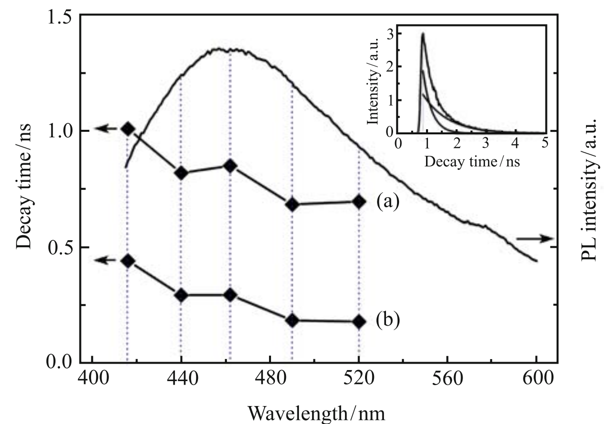


**Fig. 7** Time-resolved analysis for a PL spectrum obtained with an excitation wavelength of 375 nm, **(a)** the long decay time and **(b)** the short decay time at the specified emission wavelengths. The data result from fitting the decaying process with a double exponential decaying function, as exemplified in the inset where the decaying curve was measured for the emission at 462 nm.

## 4 Si-in-SiC compound films

Silicon carbide as an important semiconducting material possesses potential applications in high-temperature, high-power, high-frequency, and radiation-hardened fields. However, drawing light from silicon carbide has proven to be a very difficult enterprise due to the material's intrinsic indirect band gap structure. Researchers have manufactured several nanostructures such as quantum wells [18] and SiC nanocrystals [19−21] in order to engineer a direct band gap following the QCE. However, silicon particles survived in silicon carbide matrix should also emit light though SiC will constitute a rela-

tively weaker confinement. The study of light emission from the nanostructured Si-in-SiC compound films will be of essential interest in its own right [22].

Strong PL were measured in the Si-in-SiC samples thus prepared as the Si-in-$SiN_x$ films, and such a result can be equally attributed to the QCE mechanism based on the analysis of the spectral features. The known characteristic PL emissions attributed to the defects in SiC and SiC nanoparticles [23] are absent from our results. As a supportive evidence for the QCE mechanism, we noted a steady red shift of the emission in the Si-richer samples comprising enlarged silicon particles. The peak position shifts from 440 nm for sample A to 520 nm for sample C, as seen in Fig. 8. The rather large shift in the emission wavelength, $\lambda$, via a seemingly small change in the particle size, $d$, can be well understood from the viewpoint of the QCE model since it has $\Delta\lambda/\lambda = 2\Delta d/d$. A small change from 1.2 (for sample A) to 1.32 nm (for sample C) in particle size implies an increase of emission wavelength by about 20 %. This enormous shift was also observed in other systems where silicon particles of different sizes clearly exhibit quantum confined emission [24−27]. Due to the extreme smallness of the particles, the size fluctuation is expected to produce a considerably broadened profile for the confined PL emission. Therefore the labeling feature of the confined PL can be found in its broadened emission profiles, as shown in Fig. 8. The enhanced size fluctuation equally means a broadened excitation spectrum for the PL process.

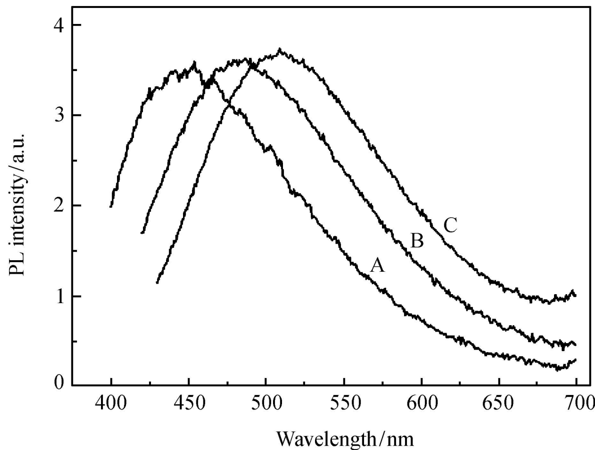


**Fig. 8** PL spectra measured in Si-in-SiC films with increasing silicon content (from A to C). Excitation wavelength: 370 nm. The peak positions are located at 450, 485, and 510 nm, respectively.

Figure 9 displays the PL curves of as-deposited Si-in-SiC film (refer to sample A) measured at different excitation wavelengths ranging from 290 to 515 nm, while no evident luminescence can be detected beyond this zone. Accordingly, the peak position, the integral intensity, and the FWHM are presented as functions of the excitation wavelength [Fig. 9(b), (c) and (d)] in order to analyze the properties of these PL profiles. In so doing, we assume a Gaussian profile for all the PL curves in Fig. 9(a), which is reasonably justifiable as stated in previous sections. In Fig. 9(b) the integral intensity is plotted against the excitation wavelength; it shows a typical binomial distribution (often fitted by a log normal distribution) in the case of small probability for each single event (here an effective excitation) [28]. The peak position of the PL spectrum is linearly correlated to the excitation wavelength at longer wavelengths, indicating a constant Stokes shift (∼1.10 eV), but deviation from linearity occurs at the first three shorter wavelengths since the corresponding photon energies surpass the band gap of the amorphous SiC matrix [Fig. 9(c)]. At the same time, the ever narrowing FWHM of the spectra, given in eV, at the longer excitation wavelength justifies once again the QCE mechanism for the PL process. It drops steadily from 0.35 to 0.16 eV [Fig. 9(d)]. This point has been discussed in detail in our previous publications concerning silicon particles embedded in $SiN_x$ matrix [24, 25, 29]. Note that the emission spectrum that extends to the violet band (below 400 nm or 3.1 eV in photon energy) loses intensity rapidly, and the corresponding photon energy has approached the band gap of the amorphous silicon carbide prepared under similar conditions ($\leqslant$3.3 eV) [30]. Therefore, we can say that the PL emission centered at 460 nm is of roughly the shortest wavelength that can be achieved in the Si-in-SiC composite structure via the quantum confinement mechanism.

The QCE mechanism for light emission from the extremely small Si particles may also indicate a very short decay time, of the order of a nanosecond, in the Si-in-SiC. Figure 10 illustrates a typical decaying process for the emission collected at the 485 nm line under the excitation of 390 nm. The decay times are obtained by fitting the decaying process with a double exponential decaying function as before. We found that, at the four chosen wavelengths for the collected emission, the decay time for the short-time attribute is 2.41 ns (390 nm), 2.63 ns (410 nm), 2.22 ns (465 nm) and 3.62 ns (505 nm), respectively. The decay time for the long-time attribute is also well below 10.0 ns. Such a short decay time, though roughly doubled as was reported on Si-in-$SiN_x$, is considerably shorter than those measured in porous silicon and in silicon particles embedded in oxide matrix. Noting that the two components of the decay time here are of the same order of magnitude, an alternative fitting using the stretched exponential function [31] seems more appropriate which, to no surprise, gives a decay time of a similar size. But again, a clear picture for

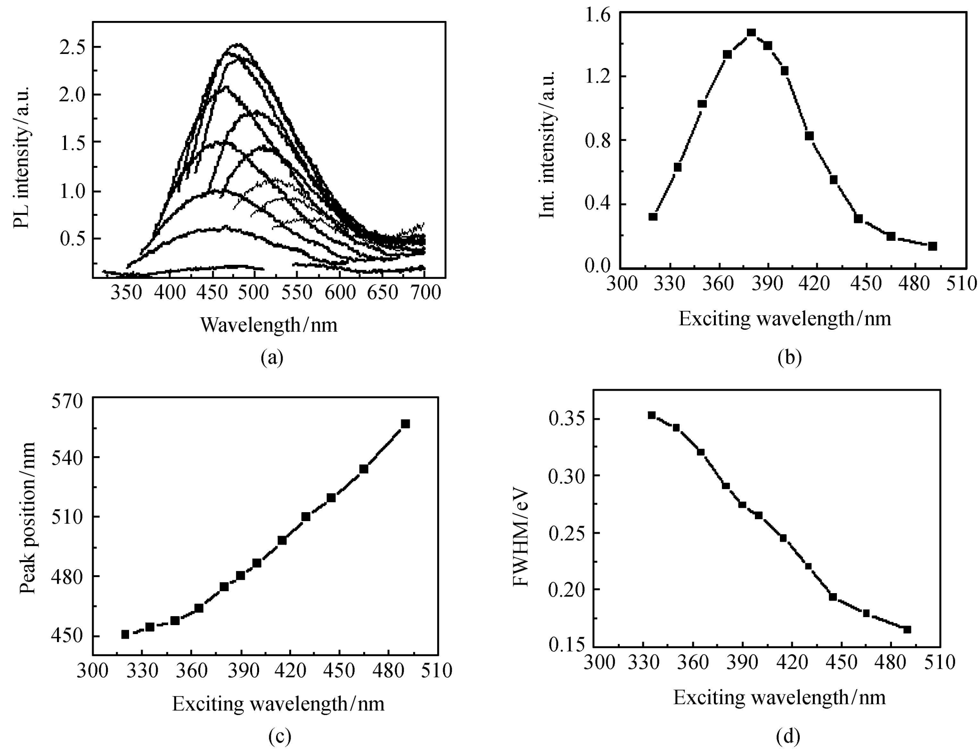


**Fig. 9** **(a)** PL profiles measured at an excitation wavelength of 290, 320, 335, 350, 365, 380, 390, 400, 415, 430, 445, 465, 490, and 515 nm (from left to right). The integral intensity, peak position and FWHM are presented as functions of the excitation wavelength in **(b)**, **(c)** and **(d)**, respectively.

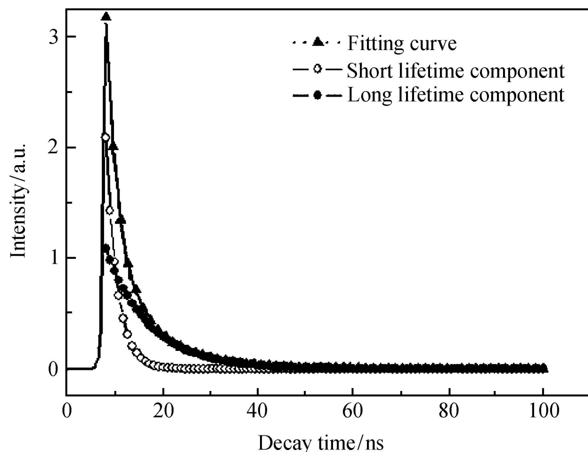


**Fig. 10** Time-resolved PL spectrum obtained with an excitation wavelength of 390 nm, and collected at the emission wavelength of 485 nm.

the underlying dynamic recombination processes is missing. This can only be resolved with more detailed measurements of the decay and excitation processes in the future.

## 5 Summary

In summary, silicon particles with an average size below 2 nm were grown onto cold substrates in amorphous $SiN_x$ and SiC matrices by employing a plasma-enhanced chemical vapor deposition procedure, which can serve as an exemplar system for the study of light emission following QCE. Strong PL extending to the violet band can be measured at room temperature, and an external quantum efficiency of over 3.0 % can be reached. The strong confinement implies a very short decay time which declines even to within 1.0 nanosecond in the Si-in-$SiN_x$ systems. The extremely small size of the silicon nanoparticles gives rise to emissions of considerably extended spectral profiles, in Si-in-SiC films comparable profiles can be obtained in one same sample with a flexible choice of excitation wavelengths. These features largely reinforce the feasibility of fabricating silicon-based nanostructured light-emitters in a procedure entirely compatible with modern very-large-scale-integration technology.

**Acknowledgements** This work was supported by the National Natural Science Foundation of China (Grant Nos. 60621091, 60306009, 10574147, and 10404034).

## References

1. L. T. Canham, Appl. Phys. Lett., 1990, 57: 1046
2. G. Ledoux, J. Gong, F. Huisken, O. Guillois, and C. Rey-

naud, Appl. Phys. Lett., 2002, 80: 4834

3. N. Satoshi, N. Keiji, and K. Yoshihiko, J. Non-Cryst. Solids, 2002, 299−302: 1095
4. A. A. Shklyaev, Y. Nakamura, and M. Ichikawa, J. Appl. Phys., 2007, 101: 033532
5. C. Marzia, W. Anja, P. Vincent, B. Caroline, C. Hubert, and C. Alain, Appl. Phys. Lett., 2005, 87: 251911
6. C. Liu, C. R. Li, A. L. Ji, L. B. Ma, Y. Q. Wang, and Z. X. Cao, Nanotechnology, 2005, 16: 1
7. I. Fabio, F. Giorgia, and S. Corrado, J. Appl. Phys., 2000, 87: 1295
8. Z. Chen, Y. X. Wang, Y. M. Zou, J. W. Wang, Y. Li, and H. J. Zhang, Appl. Phys. Lett., 2006, 89: 141913
9. K. Leonid, R. Markku, and N. Sergei, Appl. Phys. Lett., 2005, 86: 141911
10. M. L. Terranova, S. Piccirillo, V. Sessa, S. Botti, and M. Rossi, Appl. Phys. Lett., 1999, 74: 3146
11. L. B. Ma, R. Song, R. Huang, Y. Du, J. P. Ye, Y. Lin, and Y. Q. Wang, Journal of Luminescence, 2007, 126: 536
12. P. Pellegrino, A. Pe'rez-Rodriguez, B. Garrido, O. Gonza'lez-Varona, and J. R. Morante, Appl. Phys. Lett., 2004, 84: 25
13. P. D. J. Calcott, K. J. Nash, L. T. Canham, M. J. Kane, and D. Brumhead, J. Phys.: Condens. Matter, 1993, 5: L91
14. S. Ossicini, L. Pavesi, and F. Priolo, Light Emitting Silicon for Microphotonics, Berlin, Heidelberg: Springer, 2003: 172
15. T. Takagahara and K. Takeda, Phys. Rev. B, 1996, 53: R4205
16. K. Leung and K. B. Whaley, Phys. Rev. B, 1997, 56: 7455
17. H. Koyama, T. Ozaki, and N. Koshida, Phys. Rev. B, 1995, 52: R11561
18. K. Brunner, K. Eberl, and W. Winter, Phys. Rev. Lett., 1996, 69: 303
19. S. J. Xu, M. B. Yu, Rusli, S. F. Yoon, and C. M. Che, Appl. Phys. Lett., 2000, 76: 2550
20. A. Kassiba, M. Makowska-Janusik, and J. Bouclé, Phys. Rev. B, 2002, 66: 155317
21. X. L. Wu, J. Y. Fan, T. Qiu, X. Yang, G. G. Siu, and K. Chu Paul, Phys. Rev. Lett., 2005, 94: 026102
22. R. Huang, L. B. Ma, R. Song, Y. Du, H. J. Shi, J. P. Ye, Y. Lin, and Z. X. Cao, Nanotechnology, 2007, 18: 445605
23. A. O. Konstantinov, A. Henry, C. I. Harris, and E. Janz'en, Appl. Phys. Lett., 1995, 66: 2250
24. C. Liu, C. R. Li, A. L. Ji, L. B. Ma, Y. Q. Wang, and Z. X. Cao, Nanotechnology, 2005, 16: 940
25. L. B. Ma, R. Song, Y. M. Miao, C. R. Li, Y. Du, Y. Q. Wang, and Z. X. Cao, Appl. Phys. Lett., 2006, 88: 093102
26. G. Ledoux, J. Gong, F. Huisken, O. Guillois, and C. Reynaud, Appl. Phys. Lett., 2002, 80 : 4834
27. H. Rinnert, M. Vergnat, and G. Marchal, Appl. Phys. Lett., 1998, 72: 3157
28. B. Diu, C. Guthmann, D. Lederer, and B. Roulet, Éléments de Physique Statistique, Paris: Hermann, 1998
29. C. Liu, C. R. Li, A. L. Ji, L. B. Ma, Y. Q. Wang, and Z. X. Cao, Appl. Phys. Lett., 2005, 86: 223111
30. Z. Hu, X. Liao, H. Diao, G. Kong, X. Zeng, and Y. Xu, J. Cryst. Growth, 2004, 264: 7
31. J. Linnros, N. Lalic, A. Galeckas, and V. Grivickas, J. Appl. Phys., 2005, 86: 6128